Analytical interpretation and simulation of the static magnetic properties of synthetic alpha - Fe_2SiO_4

1993 J. Phys.: Condens. Matter 5 3663

(http://iopscience.iop.org/0953-8984/5/22/017)

J. Phys.: Condens. Matter 5 (1993) 3663–3672. Printed in the UK

Analytical interpretation and simulation of the static magnetic properties of synthetic α-Fe_2SiO_4*

H Ehrenberg and H Fuess

Fachgebiet Strukturforschung der Materialwissenschaft, Technische Hochschule Darmstadt, D-6100 Darmstadt, Federal Republic of Germany

Received 11 February 1993, in final form 15 March 1993

Abstract. The magnetic structure and susceptibilities of Fe_2SiO_4 were derived on the basis of localized magnetic moments. Each Fe^{2+} ion is described as a ^5D state, and crystal field, spin–orbit coupling, isotropic Heisenberg exchange, magnetic dipole–dipole interaction and external magnetic fields are taken into account. Many-particle interactions are treated in the mean-field approximation. Fundamental physical constants such as crystal-field splittings and exchange integrals are fitted to reproduce experimental results.

Within this model very good agreement between theory and experiment was obtained. It is shown that the canting of magnetic moments at inversion centres is a consequence of competition between the crystal field and strong antiferromagnetic coupling to the moments in mirror planes, each preferring different orientations. The ratio of these effects is temperature dependent and explains the evolution of the canting angle.

Further high-field magnetizations are determined and with the field in the [010] direction a field-induced phase transition and the magnetic phase diagram are predicted.

The temperature dependence of quadrupole splitting in Mössbauer experiments is also calculated and compared with experimental results.

1. Introduction

The orthosilicate α-Fe_2SiO_4 crystallizes in the olivine type structure (space group *Pnma*) and is antiferromagnetic below $T_N = 64.9$ K. Due to the non-equivalent crystallographic positions occupied by the Fe^{2+} ions, a complicated magnetic structure results. The determination of this structure was achieved by elastic neutron scattering on powders at 4 K by Santoro *et al* (1966) and on single crystals at various temperatures by Lottermoser *et al* (1986). All magnetic reflections are indexed on the crystallographic cell, i.e. this cell is also the magnetic cell ($k = 0$). While the magnetic moments on the M2 sites (local symmetry m) are collinear and parallel to [010] for all temperatures below T_N, the moments on the M1 sites (local symmetry $\bar{1}$) are canted with a canting angle decreasing with temperature (figure 1, table 1). The measured magnetic susceptibilites show pronounced anisotropy (figure 4(*a*), Ballet *et al* 1989). The maximum in c direction at 20 K is a particular challenge to a theoretical treatment. In contrast to previous publications based on effective spin Hamiltonians, we take the degrees of freedom of orbital angular momentum explicitly into account.

* Dedicated to Professor Bertaut on the occasion of his 80th birthday.

0953-8984/93/223663+10$07.50

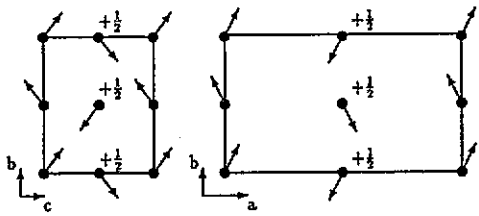

Figure 1. Projection of the canted magnetic moments in the M1 site (Fuess *et al* 1988).

Table 1. Canting angles for the M1 site and absolute values of the sublattice magnetizations at several temperatures from Fuess *et al* (1988). α, (β, γ) is the angle between the magnetic moment of ion 1 (see figure 1) and the a (b, c) axis.

T (K)	$\cos\alpha$	$\cos\beta$	$\cos\gamma$	$\|\mu\|$(M1)	$\|\mu\|$(M2)
10	0.31(2)	0.77(1)	0.57(2)	4.40(10)	4.41(5)
23	0.21(3)	0.88(2)	0.43(1)	3.40(20)	4.40(10)
35	0.25(8)	0.89(1)	0.38(7)	2.80(20)	4.10(4)
50	0.08(5)	0.96(4)	0.27(3)	2.10(20)	3.74(7)

2. The model

According to Hund's rules the $3d^6$ electron configuration for Fe^{2+} leads to a ^5D ground state. Since the first excited state is at $\nu \approx 30\,000\ cm^{-1}$, the Hilbert space for ion i is restricted to

$$\mathcal{H}^{(i)} = \{|L = 2, M_L\rangle|S = 2, M_S\rangle;\ M_L, M_S = -2, \ldots, 2\}. \tag{1}$$

In this space the following Hamiltonian has to be applied:

$$\hat{H}^{(i)} = \hat{H}^{(i)}_{\text{crystal-field}} + \hat{H}^{(i)}_{\text{spin-orbit}} + \hat{H}^{(i)}_{\text{exchange}} + \hat{H}^{(i)}_{\text{magnetic dipole-dipole}} + \hat{H}^{(i)}_{\text{Zeeman}}. \tag{2}$$

The different interactions are subsequently discussed in decreasing order of magnitude. In the case of d states a principal-axis system (PAS) for the crystal-field potential $V(r)$ may be constructed. For a free ion the five d states are degenerate. In a crystal field of cubic symmetry they are split into a low-lying triplet $^5T_{2g}$ (irreducible representation Γ_5) and a doublet ^5E_g (Γ_3) spanned by the following basis vectors quantized in PAS (angular dependence):

$$\begin{aligned}
^5E_g &: |\theta\rangle = |2, 0\rangle && (3z^2 - r^2)\\
&\quad |\epsilon\rangle = 1/\sqrt{2}(|2, 2\rangle + |2, -2\rangle) && (x^2 - y^2)\\
^5T_{2g} &: |\eta_x\rangle = i/\sqrt{2}(|2, -1\rangle + |2, 1\rangle) && (yz)\\
&\quad |\eta_y\rangle = 1/\sqrt{2}(|2, -1\rangle - |2, 1\rangle) && (xz)\\
&\quad |\eta_z\rangle = -i/\sqrt{2}(|2, 2\rangle - |2, -2\rangle) && (xy).
\end{aligned} \tag{3}$$

In a field of low symmetry the degeneracy is lifted, but the $|\eta_i\rangle$, $i = x, y, z$ still remain eigenfunctions (Moriya *et al* 1956). Crystal-field splitting in natural Fe_2SiO_4 has been examined by Burns (1970), recording polarized absorption spectra. In order to index the

observed absorption lines, he approximated the M1 sites to be of symmetry D_{4h} and the M2 sites of C_{3v}:

$$\begin{aligned}\nu(^5E_g \rightarrow {}^5A_{1g}) &\approx 8060\ \text{cm}^{-1}\\ \nu(^5E_g \rightarrow {}^5B_{1g}) &\approx 11\,060\ \text{cm}^{-1}\\ \nu(^5E \rightarrow {}^5E) &\approx 9290\ \text{cm}^{-1}.\end{aligned} \tag{4}$$

Because of this large splitting the high-lying doublet states do not contribute to magnetic properties in a significant way and the Hilbert space of (1) can be reduced to

$$\mathcal{H}^{(i)} = \{|\eta_i\rangle | S = 2,\ M_S\rangle;\ i = x, y, z;\ M_S = -2, \ldots, 2\}. \tag{5}$$

In PAS the matrix elements $\langle\eta_\alpha|\hat{L}_i|\eta_\beta\rangle = (L_i)$; $i, \alpha, \beta = x, y, z$ are calculated after (3) and differ from a non-standard representation of angular momentum $L = 1$ only by a factor $\kappa = -1$, giving rise to the concept of fictitious angular momentum (Abragam and Pryce 1951):

$$(L_x) = \kappa \begin{pmatrix} 0 & 0 & 0 \\ 0 & 0 & -i \\ 0 & i & 0 \end{pmatrix} \qquad (L_y) = \kappa \begin{pmatrix} 0 & 0 & i \\ 0 & 0 & 0 \\ -i & 0 & 0 \end{pmatrix} \qquad (L_z) = \kappa \begin{pmatrix} 0 & -i & 0 \\ i & 0 & 0 \\ 0 & 0 & 0 \end{pmatrix}. \tag{6}$$

Altogether we need eight model parameters to describe the effects of the crystal field:

- $2 + 2$ crystal-field splittings for the low-lying triplets in the two non-equivalent sites. The zero level can be choosen for the M1 and M2 sites separately: $E_1^x, E_1^y, E_1^z, E_2^x, E_2^y, E_2^z$.
- $3 + 1$ Eulerian angles to characterize the transformation from the crystal-axis system (CAS) to PAS. Due to the mirror symmetry the b direction must be one of the principal axes for the M2 sites: $\alpha_1, \beta_1, \gamma_1, \beta_2$.

As a consequence of large cubic splitting, the covalency factors κ_1 and κ_2 are kept fixed and equal to -1 in a first step. Small departures from $\kappa = -1$ take account of the admixture of the high-energy doublet (Abragam and Pryce 1951). Variations of these parameters are a suitable test for the reduction of Hilbert space as discussed above.

Using the standard representation for spin $S = 2$ quantized in PAS as well, the matrix elements of spin–orbit coupling

$$\hat{H}^{(i)}_{\text{spin–orbit}} = \lambda \hat{L} \cdot \hat{S} \tag{7}$$

in (5) are readily determined from (6). Two more model parameters λ_1 and λ_2 were introduced. In crystals the absolute value of the spin–orbit coupling constant is expected to be reduced in comparison to that of the free-ion value $\lambda_0 = -103\ \text{cm}^{-1}$ (Abragam and Bleaney 1970).

The many-particle interactions included are Heisenberg exchange and magnetic dipole–dipole interactions and these will be treated in the mean-field approximation. The operators of all ions $j \neq i$ are replaced by their thermal expectation values, resulting in a one-particle interaction with an effective field

$$\hat{H}^{(i)}_{\text{exchange}} = -\sum_{j \neq i} J_{ij} \hat{S}^{(i)} \hat{S}^{(j)} \rightarrow -\sum_{j \neq i} J_{ij} \hat{S}^{(i)} \langle S^{(j)} \rangle_T. \tag{8}$$

Table 2. Included exchange couplings for ions 1 and 5.

i	j	Exchange integral	Multiplicity
1	2	J_{12}	2
	5,6	J_{15}	1
	7,8	J_{35}, J_{53}	1
5	1,2	J_{15}	1
	3,4	J_{35}, J_{53}	1
	7	J_{57}	4

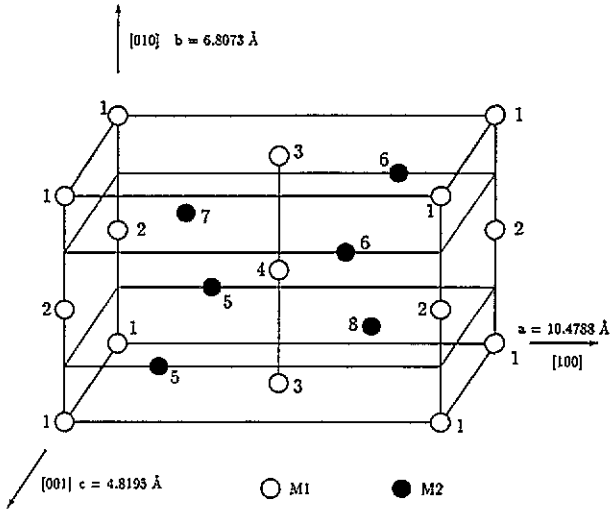

Figure 2. Indexed magnetic ions in the chemical and magnetic cell.

The included exchange integrals are listed in table 2 with the notation of figure 2 (Ballet *et al* 1987). The two non-equivalent couplings J_{35} and J_{53} only appear in the sum, so we have to deal with four more parameters: J_{12}, J_{15}, $\frac{1}{2}(J_{35}+J_{53})$ and J_{57}.

The magnetic dipole–dipole interaction can be simplified under the consideration of sublattices and translation symmetry:

$$\hat{H}^{(i)}_{\text{magnetic dipole–dipole}} = \frac{1}{4\pi\mu_0}\sum_{j\neq i}\left\{\frac{\hat{\mu}^{(i)}\hat{\mu}^{(j)}}{r_{ij}^3} - 3\frac{(\hat{\mu}^{(i)}\boldsymbol{r}_{ij})(\hat{\mu}^{(j)}\boldsymbol{r}_{ij})}{r_{ij}^5}\right\}$$
$$\rightarrow \hat{\mu}^{(i)}\sum_{j=1,\ldots,8}(\boldsymbol{H}_{ij})\langle\mu^{(j)}\rangle_T. \tag{9}$$

The geometrical quantity

$$(\boldsymbol{H}_{ij})^{\alpha\beta} = \frac{1}{4\pi\mu_0}\sum_{r\neq 0}\left(\frac{\delta^{\alpha\beta}}{r^3} - 3\frac{r^\alpha r^\beta}{r^5}\right) \tag{10}$$

depends on crystal structure and has to be calculated only once. The summation runs over all cells. Because $\mu^{(i)} = -\mu_B(2S^{(i)} + L^{(i)})$ the matrix elements can be derived as discussed above. With an external magnetic field we have an additional contribution due to the Zeeman term,

$$\hat{H}^{(i)}_{\text{Zeeman}} = -\hat{\mu}^{(i)}H_{\text{ext}}. \tag{11}$$

3. Simulation

For a given set of parameters the magnetic ordering can be found as follows. In the first step a set of thermal expectation values $\langle L^{(j)}\rangle_T^0$, $\langle S^{(j)}\rangle_T^0$; $j = 1, \ldots, 8$ can be chosen at random except the set with all expectation values vanishing. Now the matrix elements of $\hat{H}^{(i)}$, $i \in \{1 \ldots 8\}$ in the Hilbert space of (5) can be calculated and the eigenstates are found by diagonalization. In the next step the set of thermal expectation values is modified by recalculating $\langle L^{(i)}\rangle_T$, $\langle S^{(i)}\rangle_T$. This procedure is repeated for the next ion i and so on. All calculations are performed in the PAS of ion i. The magnetic structure is determined by the self-consistent solution of this iteration. To check whether this solution is unique the calculations were performed for a wide range of initial conditions. The iterations always converged to physically equivalent states.

The model parameters are fitted to magnetic moments in the ordered phase and to single-crystal susceptibilities in the whole temperature range. The results are shown in figure 3. The fundamental physical constants determining these properties are found to be

$$\begin{array}{llll} \lambda_1 \approx -78.5\ \mathrm{cm}^{-1} & E_1^x - E_1^z \approx 1960\ \mathrm{cm}^{-1} & \alpha_1 \approx -0.8 & J_{12} \approx -1.95\ \mathrm{cm}^{-1} \\ \lambda_2 \approx -81\ \mathrm{cm}^{-1} & E_1^y - E_1^z \approx 780\ \mathrm{cm}^{-1} & \beta_1 \approx 1.45 & J_{15} \approx -1.4\ \mathrm{cm}^{-1} \\ & E_2^y - E_2^x \approx 1740\ \mathrm{cm}^{-1} & \gamma_1 \approx -0.48 & \tfrac{1}{2}(J_{35} + J_{53}) \approx -4.3\ \mathrm{cm}^{-1} \\ & E_2^z - E_2^x \approx 1180\ \mathrm{cm}^{-1} & \beta_2 \approx -0.7 & J_{57} \approx -3.2\ \mathrm{cm}^{-1}. \end{array} \tag{12}$$

The sublattice magnetization for the M2 site is slightly too small at all temperatures. This is an indication that the crystal-field splitting should be smaller, leading to less quenching on the M2 site. A reduction of this parameter improves the agreement between simulation and experiment in view of the structural data, but the susceptibilities are not reproduced so well. With regard to covalency factors κ_1 and κ_2, the best correspondence is achieved with departures from -1 of less than 5%, which need not be included. This confirms the assumption that the high-energy doublets do not influence the magnetic properties.

4. Discussion

The magnetic structure of Fe_2SiO_4 is explained as follows. Strong antiferromagnetic coupling within the M2 site forces spins 5 and 7 (6 and 8) to be antiparallel. Because of a large negative coupling constant for exchange between spins 5 and 3 (6 and 3), spins 5 and 6 are parallel. The expectation value of $\hat{L}$ for the lowest crystal-field level is zero. Treating the spin–orbit coupling as a perturbation, we find that the first-order corrections on the M2 site contribute only to $\langle L_y\rangle$ ($\langle\eta_x|\hat{L}_i|\eta_z\rangle = 0$ for $i = x, z$). Terms of higher order do not alter the fact that the b axis is the preferred direction for the collinear alignment of magnetic moments in the M2 site because of the large splittings.

The situation is more complicated in the M1 site because of smaller crystal-field splitting and weaker intra-site exchange coupling. The crystal field favours orbital angular momentum to be in the z direction of the PAS; this is $R^{-1}(\alpha_1, \beta_1, \gamma_1)e_z$ in the CAS. Because of strong antiferromagnetic coupling to the ions at M2 sites, spins prefer alignment parallel to [010]. These effects are in competition due to spin–orbit coupling and lead to canting of the magnetic moments in an intermediate direction. The canting angle depends on temperature, because the competing interactions scale as $|\langle L\rangle_T(\mathrm{M1})| \cdot |\langle S\rangle_T(\mathrm{M1})|$ and

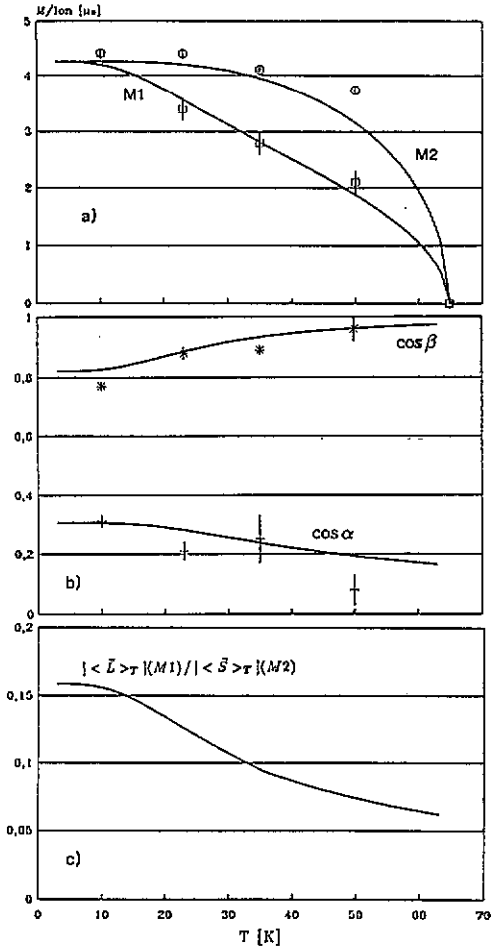

Figure 3. Sublattice magnetizations (*a*) and canting angles (*b*) as function of temperature (full curves, simulation; symbols, experimental data of Fuess *et al* (1988)). The ratio in (*c*) is mainly responsible for the temperature dependence of the canting angle (see text).

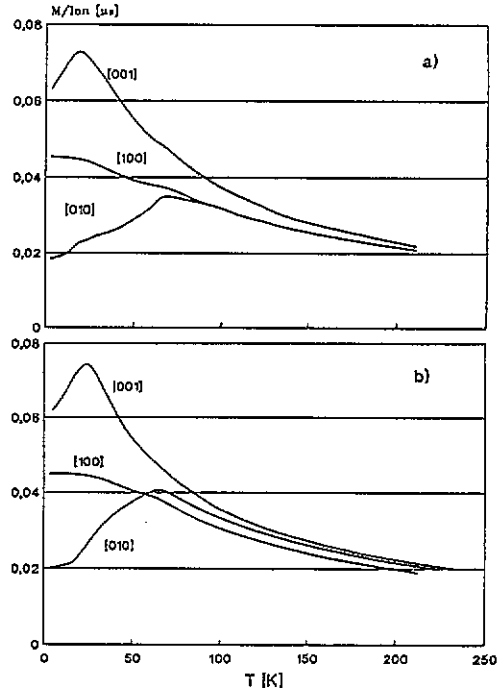

Figure 4. Single-crystal magnetizations per ion with an external magnetic field of $H = 10$ kOe: (*a*) experiment (*b*) simulation.

$|\langle S\rangle_T(\mathrm{M1})| \cdot |\langle S\rangle_T(\mathrm{M2})|$ respectively. In table 3 the absolute thermal expectation values are listed for several temperatures. Figure 3(*c*) shows the ratio of $|\langle L\rangle_T(\mathrm{M1})|/|\langle S\rangle_T(\mathrm{M2})|$ as a function of temperature. The decrease of this ratio indicates a predominant role of exchange and as a consequence the magnetic moments are turned into the *b* direction.

Table 3. Thermal expectation values for angular momentum at several temperatures obtained from simulation.

T (K)	3	18	30	48	63
$\lvert\langle S\rangle_T\rvert$(M1)	1.976	1.815	1.478	0.961	0.312
$\lvert\langle L\rangle_T\rvert$(M1)	0.317	0.277	0.204	0.118	0.036
$\lvert\langle S\rangle_T\rvert$(M2)	1.993	1.985	1.912	1.553	0.581
$\lvert\langle L\rangle_T\rvert$(M2)	0.269	0.268	0.258	0.210	0.030

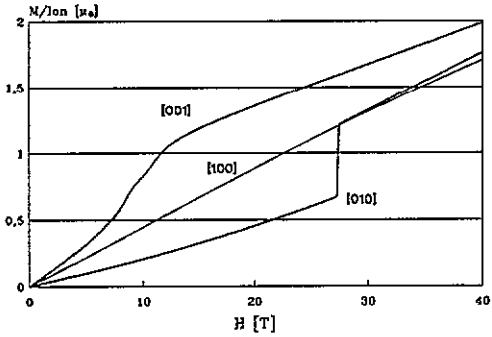

Figure 5. Magnetization per ion with the field in different crystallographic directions at $T = 4.2$ K (simulation).

Furthermore, the high-field magnetizations are determined (figure 5). With the magnetic field parallel to [010] a field-induced phase transition is predicted. The critical magnetic field strength H_c depends on temperature, leading to the magnetic phase diagram of figure 6. The phase transition can be characterized by a switch of the magnetic moments into the c direction, conserving antiferromagnetism between spins to a large extent. Alignment in the c direction is favoured by the magnetic dipole–dipole interaction, but without an external magnetic field the magnetic moments are forced into the b direction due to the crystal field. Parallel to [100] we find a small ferromagnetic component within both sites, but of opposite sign. For the compound Co_2SiO_4 two phase transitions were determined experimentally and were calculated by Brotzeller *et al* (1992) from a spin-wave model. Investigations are made for Fe_2SiO_4 as well. The intermediate phase, corresponding to a switch of magnetic moments on the M1 site alone, seems to be unstable within our model parameters. In other directions no phase transitions occur.

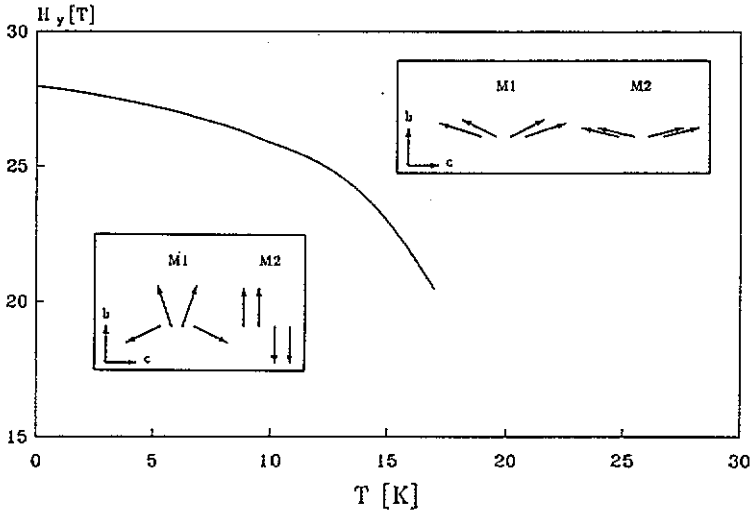

Figure 6. Magnetic phase diagram with the field in the [010] direction and a schematic representation of the two different phases.

The specific heat C_m of the magnetic system is calculated by considering the increase $\delta E(T)$ in its energy $E(T)$, when the temperature T increases by δT: $C_m = \delta E(T)/\delta T$. We find a satisfactory qualitative description of the behaviour reported by Robie *et al*

(1982), in particular the shoulder at 20 K is reproduced (figure 7). Near to the phase transition quantitative discrepancy is not surprising because of the inadequacy of the mean-field approximation for dynamics of critical phenomena.

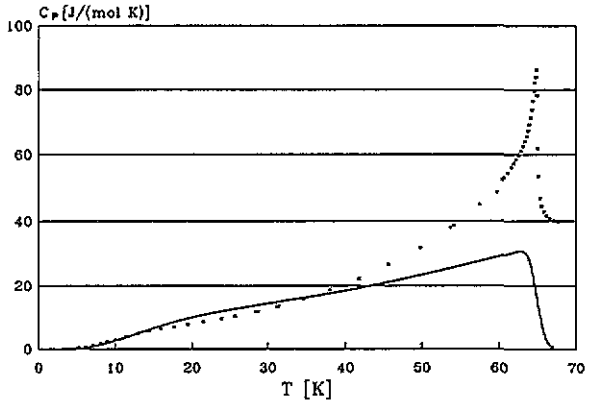

Figure 7. Measured specific heat (Robie *et al* 1982) in comparison to the calculated magnetic contribution.

Additional information about crystal-field splittings Δ_1, Δ_2 is available from the temperature dependence of quadrupole splitting in Mössbauer experiments. We used the method of Ingalls (1964) to calculate the reduction function $F(\Delta_1, \Delta_2, \lambda, T)$ for the M1 and M2 sites using (12). The results are shown in figures 8 and 9 confirming the temperature independence below T_N for both sites within experimental error as reported by Lottermoser (1986) in contrast to the work by Hafner *et al* (1990).

Measurements at higher temperatures were carried out by Eibschütz and Ganiel (1967) and are reported in figure 9. Their data have been evaluated by Huggins (1976), who used the simplified method of Ingalls neglecting spin–orbit coupling. He derived splittings $\Delta_1 \approx 710\,\mathrm{cm}^{-1}$, $\Delta_2 \approx 1500\,\mathrm{cm}^{-1}$ for the M1 site and $\Delta_1 \approx 620\,\mathrm{cm}^{-1}$ and $\Delta_2 \approx 1400\,\mathrm{cm}^{-1}$ for the M2 site. Because of large uncertainty these values for the M2 site have been questioned by Burns (1984) and were replaced by $\Delta_1 \approx \Delta_2 \approx 1670\ \mathrm{cm}^{-1}$ in accordance with absorption spectra. With these changes we agree that the lower quadrupole splittings belong to the M1 site, in contrast to the interpretation of Huggins.

The overestimation for the M2 site at higher temperatures is an additional indication of a too large crystal-field splitting at this site in our model.

5. Summary

We are able to explain the static magnetic properties and thermal behaviour of Fe_2SiO_4 in terms of fundamental physical quantities. The magnetic structure below T_N and susceptibility data were used to determine their values. While the spin–orbit coupling constant is quenched by about approximately 20% with regard to the free-ion value for both sites, stronger exchange coupling within the M2 site prohibits canting of spins, in contrast to the M1 site.

The quenching of orbital angular momentum is not complete, giving rise to a competition of crystal-field anisotropy and antiferromagnetic exchange via spin–orbit coupling. The ratio of these interactions scales as $|\langle L\rangle_T(\mathrm{M1})|/|\langle S\rangle_T(\mathrm{M2})|$ and explains the evolution of canting angle with temperature for the magnetic moments at inversion centres.

Crystal-field splittings are found to be $\Delta_1 \approx 1960\ \mathrm{cm}^{-1}$ and $\Delta_2 \approx 780\ \mathrm{cm}^{-1}$ for the M1 site and $\Delta_1 \approx 1740\ \mathrm{cm}^{-1}$ and $\Delta_2 \approx 1180\ \mathrm{cm}^{-1}$ for the M2 site. This is of

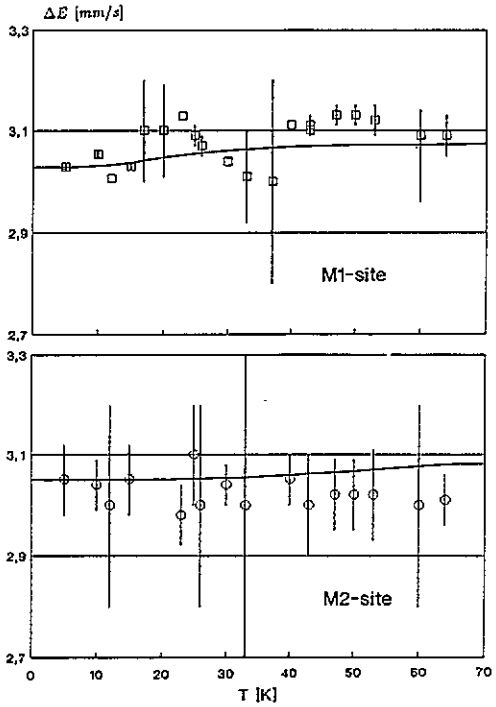

Figure 8. Quadrupole splittings in Mössbauer experiments for the M1 and M2 sites in the antiferromagnetic phase (full curves, simulation; symbols, experimental data of Lottermoser (1986)).

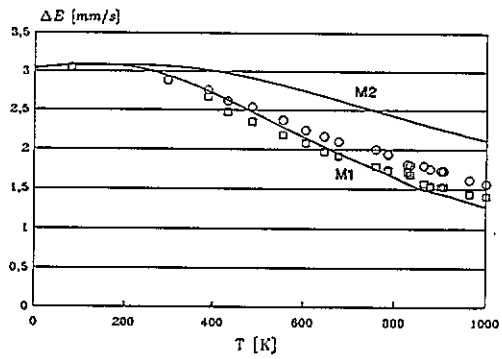

Figure 9. As figure 8, but for the high-temperature range (full curves, simulation; symbols, experimental data of Eibschütz *et al* (1967)).

reasonable order in comparison to the values reported by Burns from polarized absorption spectra and by Huggins from the temperature dependence of the quadrupole splitting in Mössbauer experiments. Nevertheless there are signs that crystal-field splitting for the M2 site is overestimated.

Acknowledgment

Support of this work by the Bundesminister für Forschung und Technologie (grant 03–FU3DAR) is gratefully acknowledged.

References

Abragam A and Bleaney B 1970 *Electron Paramagnetic Resonance of Transition Ions* (Oxford: Clarendon)

Abragam A and Pryce M H L 1951 *Proc. R. Soc.* A **205** 135–53

Ballet O, Fuess H and Fritzsche T 1987 *Phys. Chem. Minerals* **15** 54–8

Ballet O, Fuess H, Wacker K, Untersteller E, Treutmann W, Hellner E and Hosoya S 1989 *J. Phys.: Condens. Matter* **1** 4955–70

Brotzeller C, Jaitner H, Hock B, Neumann O, Geick R, Treutmann W, Hosoya S and Kato H 1992 *J. Magn. Magn. Mater.* **104–107** 949–50

Burns R G 1970 *Am. Mineral* **55** 1608–32

—— 1984 *Rev. Mineral.* **14** 277–316

Eibschütz M and Ganiel U 1967 *Solid State Commun.* **5** 267–70
Fuess H, Ballet O and Lottermoser W 1988 *Structural and Magnetic Phase Transitions in Minerals* ed S Ghose, J M Coey and E Salje (Berlin: Springer) pp 185–207
Hafner S S, Stanek J and Stanek M 1990 *J. Phys. Chem. Solids* **51** 203–8
Huggins F E 1976 *The Physics and Chemistry of Minerals and Rocks* ed. R G J Strens (New York: Wiley) pp 613–40
Ingalls R 1964 *Phys. Rev.* A **133** 787–95
Lottermoser W 1986 *Thesis* Universität zu Frankfurt am Main
Lottermoser W, Müller R and Fuess H 1986 *J. Magn. Magn. Mater.* **54–57** 1005–6
Moriya T, Motizuki K, Kanamori J and Nagamiya T 1956 *J. Phys. Soc. Japan* **11** 211–25
Robie R A, Finch C B and Hemingway B S 1982 *Am. Mineral* **67** 463–9
Santoro R P, Newnham R E and Nomura S 1966 *J. Phys. Chem. Solids* **27** 655–6